

Elliptically polarized Jovian decametric radiation: An investigation of the electron cyclotron maser mechanism

A. J. Willes, D. B. Melrose, and P. A. Robinson

Department of Theoretical Physics and Research Center for Theoretical Astrophysics, School of Physics, University of Sydney, Australia

Abstract. A model for the elliptical polarization of Jovian decametric radiation is presented, based on the electron cyclotron mechanism. The aim is to determine whether the observed elliptical polarization is consistent with the radiation being generated by mildly relativistic electrons streaming along converging magnetic field lines. The growth rate for electron cyclotron maser emission is considered, assuming a drifting DGH distribution function for the streaming electrons. Constraints on the allowable parameters of this distribution function are made by the observed polarization, timescale, bandwidth, and angular range of the radiation.

1. Introduction

The recently observed elliptical polarization from the 10-related subsources of Jovian decametric radiation [Dulk *et al.*, 1991; Lecacheuz *et al.*, 1991; Melrose and Dulk, 1991] is not expected on the basis of the favored mechanism of electron cyclotron maser emission (ECME) from a loss cone distribution of electrons [Goldreich and Lynden-Bell, 1969; Wu and Lee, 1979]. Existing treatments of ECME [e.g., Melrose *et al.*, 1982; Omididi and Gurnett, 1982; Melrose, 1986] imply emission in the \mathbf{z} mode close to perpendicular to the magnetic field lines, in which case approximately linear polarization is expected. Elliptical polarization may be described in terms of the axial ratio T of the polarization ellipse, with $T > 0$ ($T < 0$) corresponding to a right- (left) hand sense and with $|T|$ equal to the axial ratio of the two transverse components of the electric field vector. Radiation in the \mathbf{z} mode at near-perpendicular angles has $|T| \ll 1$, so that $|T| \ll 1$ is expected for ECME.

The observed axial ratio T for the 10-related sources 10-A to Io-D is shown in Table 1 [Dulk *et al.*, 1994, 1991; Lecacheuz *et al.*, 1991; Barrow, 1992], with sources Io-B and Io-C exhibiting both left- and right-handed polarizations. The handedness of the polarization is interpreted as \mathbf{z} mode radiation from the northern (right-hand sense) and southern (left-hand sense) Jovian hemispheres, at the cyclotron frequency [Dulk *et al.*, 1991]. The separated left- and right-hand polarizations for the Io-B and Io-C sources correspond to emission from different hemispheres. It is apparent that the emission from the southern hemisphere is more circularly polarized.

From the theory of ECME the emission is predicted to be confined to the surface of a hollow cone centered on the magnetic field direction [Hewiit *et al.*, 1981, 1982], and there is observational support for this for Jovian decametric emission [Dulk, 1967; Goldstein and Thieman, 1981]. To a first approximation, ECM radiation in the \mathbf{x} mode is predicted to have an axial ratio T related to the angle of emission θ via $T \approx |\cos\theta|$ [Melrose and Dulk, 1993], where θ is the angle between the magnetic field \mathbf{B} and the wave vector \mathbf{k} . A further result from the theory is that θ is related to the typical speed v of the electrons parallel to the field lines that generate the emission, through $|\cos\theta| \approx v/c$ [Hewiit *et al.*, 1982]. Thus the different axial ratios in different subsources suggest that the electrons that generate the emission have a characteristic speed (along the field lines) which is fixed for each subsource, and varies from one subsource to another. However, the relation $T \approx |\cos\theta| \approx v/c$ is derived for nonrelativistic electrons, with $v/c \ll 1$ (applicable to loss cone distributions with low energy electrons), and the assumption that the electrons are nonrelativistic appears not to be valid here. Our purpose in this paper is to generalize this theory of ECME to moderately relativistic distributions of electrons, in order to explain the elliptical polarization of the Jovian emission. The observed axial ratio, timescale, and bandwidth of the Jovian S bursts (and to a lesser extent, the more prevalent L bursts) are used to constrain the parameters of the assumed distribution function.

A useful pictorial technique for describing ECME is to plot the distribution function in normalized momentum space (with axes u_{\parallel} and u_{\perp} , which are the components of $\mathbf{u} = \gamma\mathbf{v}/c = \mathbf{p}/(mc)$, parallel and perpendicular to the magnetic field). One then considers the curve in this space defined by the condition for electrons to be in resonance with a given wave (given ω and θ). The corresponding curve in velocity ($v_{\parallel} - v_{\perp}$ space) is called a resonance ellipse [Hewiit *et al.*, 1981, 1982] for $|n_{\parallel}| = \mu|\cos\theta| \leq 1$ (where μ is the refractive index)

Copyright 1994 by the American Geophysical Union.

Paper number 94JA01843.
0148-0227/94/94JA-01843\$05.00

Table 1. Axial Ratio and Derived Angle of Emission and Drift Velocity for Each Source

Source	T	θ_{\max}	v_d/c
Io-A	-0.42	42°	0.48
Io-B	-0.26	50°	0.45
Io-B	+0.56	35°	0.49
Io-C	-0.38	44°	0.47
Io-C	+0.58	34°	0.49
Io-D	+0.52	37°	0.49

and is a hyperbola for $|n_{\parallel}| > 1$. The growth rate of a particular wave is determined by an appropriate integral around this curve. Wave growth can be due to a positive gradient either in u_{\perp} ($\partial f/\partial u_{\perp} > 0$) or in u_{\parallel} ($\cos\theta \partial f/\partial u_{\parallel} > 0$). The standard version of ECME [Wu and Lee, 1979; Melrose, 1986] relies on the perpendicular gradient in velocity. The alternative parallel-gradient driven maser for nonrelativistic electrons requires an extreme temperature anisotropy in the distribution function [Melrose, 1986].

In section 2 the analytic form for the growth rate for electron cyclotron maser emission from a spiraling beam distribution function is considered in the context of the Jovian emission. In section 3 a semiquantitative theory for the growth rate is developed, and in section 4 this theory is used to determine the typical parameters of the distribution function consistent with the emission.

2. Theory

In this section an explicit form of the growth rate for electron cyclotron maser emission from a drifting DGH distribution function is given, based on the results of Willes and Robinson [1994].

2.1. Resonance Ellipse in $u_{\parallel} - u_{\perp}$ Space

The wave-particle resonance condition for a wave with frequency ω , wavevector \mathbf{k} , and an electron with normalized momentum \mathbf{u} in a magnetized plasma is [Melrose, 1986]

$$\gamma\omega - s\Omega_e - kc u \cos\theta \cos\alpha = 0, \quad (1)$$

where Ω_e is the electron cyclotron frequency, $\gamma = (1 - v^2/c^2)^{-1/2}$ is the Lorentz factor, s is the harmonic number, θ is the wave angle defined above, and α is the pitch angle of the particle. The resonance condition (1) defines a resonance ellipse in $u_{\parallel} - u_{\perp}$ space, in the case $|n_{\parallel}| = \mu|\cos\theta| < 1$ relevant here. The semimajor axis u_R , which is parallel to the u_{\parallel} axis, the eccentricity e , and center u_0 , which is on the u_{\parallel} axis, are given by

$$u_R = \frac{\sqrt{(s\Omega_e/\omega)^2 + n_{\parallel}^2} - 1}{1 - n_{\parallel}^2}, \quad (2)$$

$$e = n_{\parallel}, \quad (3)$$

$$u_0 = \frac{s\Omega_e n_{\parallel}}{\omega(1 - n_{\parallel}^2)}, \quad (4)$$

respectively. This is in contrast with resonance ellipses in velocity space [e.g., Melrose et al., 1982], which are ellipses with the major axis parallel to the u_{\perp} axis. For perpendicular propagation ($\theta = 90^\circ$), the resonance ellipse is a circle centered on the origin. As θ decreases, the center of the ellipse moves to the right (increasing u_{\parallel}) and the eccentricity increases. As ω decreases, the ellipse becomes larger.

2.2. Growth Rate

The growth rate Γ_M for ECME, defined so that the energy in the waves grows as $e^{\Gamma_M t}$ [Melrose, 1986], is

$$\Gamma_M(\mathbf{k}, s) = \sum_{s=-\infty}^{\infty} \frac{\hbar}{mc} \int d^3\mathbf{u} w_M(\mathbf{k}, \mathbf{u}, s) \times \left(\frac{s\Omega_e}{cu_{\perp}} \frac{\partial}{\partial u_{\perp}} + k_{\parallel} \frac{\partial}{\partial u_{\parallel}} \right) f(\mathbf{u}), \quad (5)$$

where $f(\mathbf{u})$ is the distribution function of the electrons and M refers to the wave mode. The two derivative terms in (5) correspond to the parallel and perpendicular gradients in the velocity distribution, and their net effect is required to be positive for growth to occur. The factor $w_M(\mathbf{k}, \mathbf{u}, s)$ has the form [Melrose, 1986],

$$w_M(\mathbf{k}, \mathbf{u}, s) = \frac{2\pi q^2 R_M(\mathbf{k})}{\epsilon_0 \hbar |\omega_M(\mathbf{k})|} |\mathbf{e}_M^*(\mathbf{k}) \cdot \mathbf{V}(\mathbf{k}, \mathbf{u}, s)|^2 \gamma \times \delta(\gamma\omega - s\Omega_e - k_{\parallel} c u_{\parallel}), \quad (6)$$

where the ratio of electric to total energy $R_M(\mathbf{k})$, the dispersion relation $\omega_M(\mathbf{k})$, and the polarization vector $\mathbf{e}_M(\mathbf{k})$ fully describe the wave mode M . The delta function in (6) has the resonance condition (1) as its argument, so that the growth rate (5) may be evaluated as an integral along the resonance ellipse in $u_{\parallel} - u_{\perp}$ space.

The chosen distribution function $f(\mathbf{u})$ must satisfy the requirement that the electrons stream with a nonzero mean velocity along the field lines and also have regions where the u_{\parallel} or u_{\perp} gradient is positive. This distribution is modeled using a DGH distribution [Dory et al., 1965] shifted along the u_{\parallel} axis so that the electrons stream with a mean drift normalized momentum u_d ,

$$f(\mathbf{u}) = \frac{n_b}{j!(2\pi)^{\frac{3}{2}} U^3} \left(\frac{u_{\perp}^2}{2U^2} \right)^j \times \exp \left\{ - \frac{[(u_{\parallel} - u_d)^2 + u_{\perp}^2]}{2U^2} \right\}, \quad (7)$$

where n_b is the number density of electrons in this streaming distribution, and U is the characteristic spread in u . The anisotropy in the distribution is produced by the factor u_{\perp}^{2j} , which shifts the peak of the distribution from $(u_{\parallel}, u_{\perp}) = (u_d, 0)$ to $(u_{\parallel}, u_{\perp}) = (u_d, U\sqrt{2j})$. The thermal spread is mainly dependent on U , with the perpendicular spread of the distribution decreasing with increasing j .

2.3. Approximations

The approximations made in the derivation of the growth rate [Willes and Robinson, 1994] are the **semirelativistic** approximation to the Lorentz factor, and the small gyroradius approximation to the **Bessel** functions. The **semirelativistic** approximation corresponds to setting

$$\gamma \approx 1 + \frac{u_{\parallel}^2}{2} + \frac{u_{\perp}^2}{2}, \quad (8)$$

which geometrically corresponds to approximating the resonance ellipse by a resonance circle. The resonance circle has radius and center (on the u_{\parallel} axis), derived by substituting the approximate expression (8) into the resonance condition (1)

$$u_R = \sqrt{\frac{2s\Omega_e}{\omega} + n_{\parallel}^2} - 2, \quad (9)$$

$$u_0 = n_{\parallel}. \quad (10)$$

The small gyroradius approximation corresponds to replacing the **Bessel** functions, which appear in the **integrand** of the growth rate (5), by the first term in their power series expansion.

Also necessary for the evaluation of the growth rate is the dispersion relation of the emitted waves. For simplicity, we assume that the waves satisfy $\mu = 1$, rather than using the full magnetoionic dispersion relation. In the low-density plasma in the Jovian magnetosphere, setting $\mu = 1$, as we do here, may well be a better approximation than using the magnetoionic theory. This is because the thermal spread washes out the resonance-stopband-cutoff in the z mode and x mode branches when the thermal speed satisfies [Robinson 1986b, 1987]

$$V^2/c^2 \gtrsim \omega_p^2/\Omega_e^2, \quad |\cos\theta| \gg V/c, \quad (11a)$$

$$V^2/c^2 \gtrsim (\omega_p^2/\Omega_e^2)^2, \quad |\cos\theta| \ll V/c. \quad (11b)$$

We ignore new modes and other relativistic corrections to magnetoionic dispersion for a hot distribution of electrons [Robinson, 1986b, 1987; Winglee, 1983, 1985; Pritchett, 1984; Strangeway, 1985, 1986; Le Quéau and Louam, 1989]. The condition $\omega_p/\Omega_e \ll 1$ is easily satisfied with the low number density of electrons in the source region (estimated to be $n_b \lesssim 5 \times 10^6 \text{ m}^{-3}$ [Lecacheuz et al., 1991; Melrose and Dulk, 1991; Warwick and Dulk, 1964] and the strong magnetic field ($B \approx 1 \times 10^{-3} \text{ T}$).

2.4. Numerical Results

The final form of the growth rate was derived by Willes and Robinson [1994]. A simplified form, appropriate here where the emission is close to the cyclotron frequency with $\mu = 1$, is given in Appendix A. A contour plot of the growth rate for a drifting DGH distribution is shown in Figure 1 as a function of the emission frequency and angle, with typical parameters, $u_d = 0.5$, $U = 0.2$, and $j = 2$. The frequency ω_{\max} and angle θ_{\max} at which maximum growth occurs are indicated in Figure 1. For constant θ , absorption (dashed con-

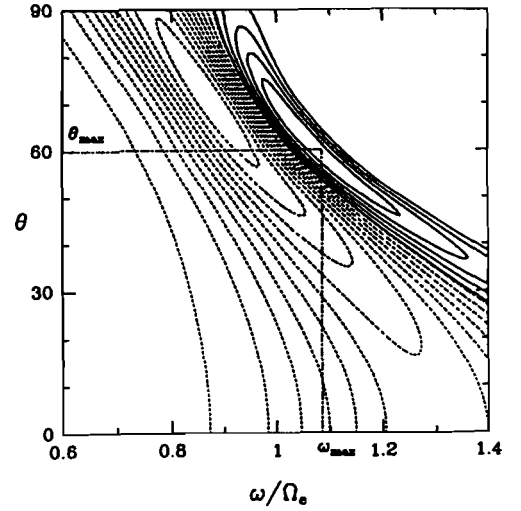


Figure 1. The growth rate Γ/Ω_e (solid contours are positive, dashed contours negative) as a function of ω and θ for $u_d = 0.5$, $j = 2$ and $U = 0.2$. The frequency ω_{\max} and the angle θ_{\max} for the maximum growth rate are shown. The maximum growth rate is $\Gamma_{\max} = 2.4 \times 10^{-4} \Omega_e$. Spacing of contours = $\Gamma_{\max}/5$.

tours) occurs at lower frequencies than growth (solid contours). The regions of growth and absorption in Figure 1 broaden with increasing U .

We define the resonance circle for maximum growth to be the particular circle corresponding to the maximum growth rate Γ_{\max} obtained at $(\omega_{\max}, \theta_{\max})$ in Figure 1. The resonant circle for maximum growth in this case is shown with the drifting DGH distribution in $u_{\parallel} - u_{\perp}$ space in Figure 2. The center of the resonance circle lies almost directly beneath the peak in the distribution function (at $u_{\parallel} = u_d$). Hence the growth due to the perpendicular gradient dominates over the growth due to the parallel gradient (see equation (5)). This is because the resonance ellipse passes through the regions of $u_{\parallel} - u_{\perp}$ space where $\partial f/\partial u_{\perp}$ is large and positive. If the growth due to the parallel gradient were important, the resonance circle would be displaced to the left of the peak of the distribution, where $\partial f/\partial u_{\parallel}$ is positive.

3. Semiquantitative Theory

Because of the complexity of the expression (A1) for the growth rate, it is desirable to have simpler expressions for the value of the maximum growth rate Γ_{\max} , the frequency ω_{\max} , and angle θ_{\max} at which maximum growth occurs. Consider the region in $\omega - \theta$ space, of width $\Delta\omega$ and $\Delta\theta$ about $(\omega_{\max}, \theta_{\max})$, where the growth rate is sufficiently high for the waves to grow substantially, say 10 e-folding growths ($\Gamma_{\max} t = 10$) [Hewitt et al., 1982]. The waves which are more than one e-folding below this maximum may be neglected. That is, $\Delta\omega$ and $\Delta\theta$ are defined by the values of ω and θ for which $\Gamma \geq 0.9 \Gamma_{\max}$. In this section, semiquantitative expressions for Γ_{\max} , ω_{\max} , θ_{\max} , $\Delta\omega$, and $\Delta\theta$ are obtained.

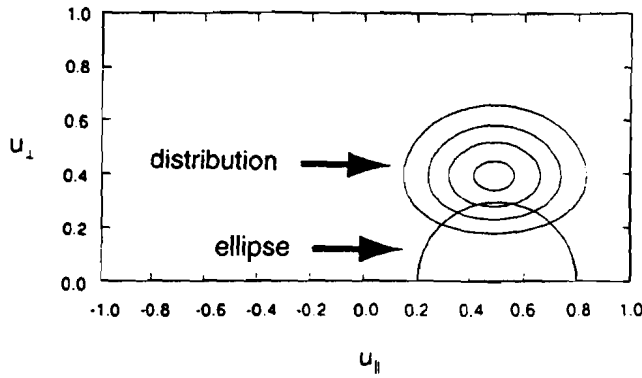


Figure 2. The resonant circle corresponding to maximum growth in Figure 1, superposed on the drifting DGH distribution function (represented as contours of $f(u)$) in $u_{\parallel} - u_{\perp}$ space.

3.1. Maximum Growth Rate

To simplify the derivation of Γ_{\max} , we approximate the position of the resonance circle for maximum growth. From Figure 2 the center of the resonance circle for maximum growth lies almost directly beneath the peak in the distribution function and the circle nearly passes through the peak itself. This is a general feature, due to the dominance of the perpendicular velocity gradient term in the growth rate (3). Hence we assume that the resonance circle for maximum growth passes through the peak of the distribution function at $(u_{\parallel}, u_{\perp}) = (u_d, U\sqrt{2j})$, giving $u_0 = u_d$ and $u_R = U\sqrt{2j}$. In fact, this gives a slight overestimation of the radius of the resonance circle, corresponding to an underestimation of Γ_{\max} .

The position of the center of the resonance circle for maximum growth implies that θ_{\max} can be determined from u_d , with

$$\theta_{\max} \approx \cos^{-1}(u_d). \quad (12)$$

Similarly, ω_{\max} can be determined from the fixed radius of the resonance circle, using (9),

$$\omega_{\max} = \frac{2\Omega_e}{2 + u_{\max}^2 - \cos^2 \theta_{\max}}, \quad (13)$$

where the fixed radius satisfies $u_{\max} = U\sqrt{2j}$ and θ_{\max} is determined from (12). Therefore, with increasing drift, θ_{\max} decreases and ω_{\max} increases.

With $(\omega_{\max}, \theta_{\max})$ now known the maximum growth rate Γ_{\max} can be estimated by integrating around the fixed resonance circle. The details are outlined in Appendix B. Our final expression for the semiquantitative growth rate is

$$\begin{aligned} \Gamma_{\max} \approx & \frac{\sqrt{\pi} \omega_{\max} \omega_p^2 2^{2j} j^{j+3/2} j! e^{-j}}{(1 + \cos^2 \theta_{\max}) \Omega_e^2 U^2 (2j + 1)!} \\ & \times \left\{ \frac{\Omega_e}{\omega} \left(\alpha^2 + \frac{u_{\max}^2 \cos^2 \theta_{\max}}{2j + 3} \right) - \frac{2(j + 1)}{2j + 3} \right. \\ & \left. \times (1 - \cos \theta_{\max} u_d) \left(a^2 + \frac{u_{\max}^2 \cos^2 \theta_{\max}}{2j + 3} \right) \right\}, \quad (14) \end{aligned}$$

where a is a parameter of order unity, cf. (A4) in Appendix A.

3.2. Bandwidth and Angular Range

The effective growth region with bandwidth $\Delta\omega$ and angular range $\Delta\theta$, as defined above, is shown in Figure 3 for the same parameters as used in Figure 1. The relation between the bandwidth $\Delta\omega$ and the angular range $\Delta\theta$ can be found by obtaining the orientation of the constant growth contours in Figure 3. This is done by differentiating (9) for the radius of the resonance circle to find the slope $d\theta/d\omega$ at $(\omega_{\max}, \theta_{\max})$,

$$\frac{d\theta}{d(\omega/\Omega_e)} = - \frac{(u_{\max}^2 - \cos^2 \theta_{\max} + 2)^2}{2 \sin 2\theta_{\max}}. \quad (15)$$

A semiquantitative estimate of $\Delta\theta$ can be obtained by assuming a linear relation between the width of the distribution and the angular range of the effective growth region, $\Delta\theta \propto U$. The dependence of $\Delta\theta$ on the perpendicular displacement of the distribution ($\propto j$) is more complicated. Here we assume a power law dependence on j , determined empirically. A linear fit using the growth rate from section 2 gives

$$\Delta\theta \approx 75 j^{0.3} U. \quad (16)$$

A semiquantitative estimate for the bandwidth can be obtained using (15) and (16), using $\Delta\omega \approx (d\omega/d\theta)\Delta\theta$.

4. Application to Jovian Decametric Radiation

In this section the minimum growth rate required to account for the observed timescale, bandwidth and range of angles for the Jovian S bursts is obtained. The constraints which apply to the longer timescale L bursts are also discussed. This information is used to determine the typical parameters for a drifting DGH distribution consistent with the observed emission. The effect of varying the chosen values of the physical parameters is then discussed.

4.1. Determination of the Mean Drift Velocity

Here we derive an expression for the characteristic drift velocity of each electron distribution contributing to the 10-related emission in terms of the observed axial ratio for that source (see Table 1). As the observed axial ratio is the same for S bursts and L bursts, the inferred drift velocity is also the same. For gyroemission the exact expression for the axial ratio T (with harmonic number $s = 1$) is [Melrose and Dulk, 1991]

$$T = \frac{(\cos \theta - \beta \cos \alpha) J_1(x)}{\beta \sin \alpha \sin \theta J_1'(x)}, \quad (17)$$

with

$$x = \frac{\beta \sin \alpha \sin \theta}{1 - \beta \cos \alpha \cos \theta}, \quad (18)$$

where α is the pitch angle and $\beta = v/c$, so that $\beta \cos \alpha =$

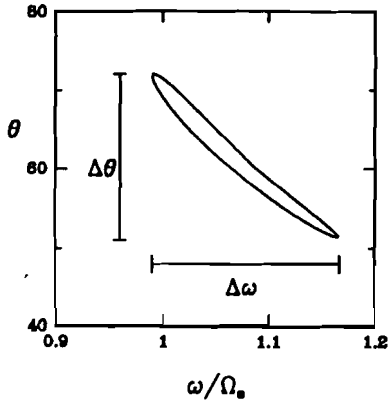


Figure 3. The region in $w - \theta$ space satisfying $\Gamma > 0.9\Gamma_{\max}$ defining the bandwidth $\Delta\omega$ and the angular range $\Delta\theta$ for the same parameters and on the same scale as Figure 1.

v_{\parallel}/c . For small x the approximation $J_1'(x) \approx J_1(x)/x$ applies, and then (17) gives

$$T \approx \frac{\cos \theta_{\max} - v_{\parallel}/c}{1 - v_{\parallel} \cos \theta_{\max}/c}. \quad (19)$$

The key result required from the theory developed in section 3 is that the resonance ellipse for maximum growth lies directly beneath the peak of the distribution function. Hence the drift velocity of the distribution satisfies

$$v_d/c \approx \frac{\cos \theta_{\max}}{1 + \cos^2 \theta_{\max}}, \quad (20)$$

where the expression on the right is the position of the center of the resonance ellipse in $v_{\parallel} - v_{\perp}$ space [Melrose and Dulk, 1993]. It is this velocity that makes the strongest contribution to the observed axial ratio (19). Substituting (20) into (19), with $v_{\parallel} = v_d$, yields the following relation between the axial ratio and the angle of emission,

$$T \approx \cos^3 \theta_{\max}, \quad (21)$$

from which the drift velocity of the distribution is determined. The angle of emission and drift velocity, derived from the observed axial ratios in Table 1 for the 10-related sources, are also given in Table 1. Note that the result $T \approx \cos \theta$ [Melrose and Dulk, 1991, 1993] for $\beta \ll 1$ is not valid for drifting distributions, as $\beta \cos \alpha$ is comparable to $\cos \theta$ in (19).

4.2. Determination of the Characteristic Distribution Width

Constraints may be placed on the characteristic distribution width U by considering the growth rates that are consistent with the polarization, timescale, bandwidth, and angular range of the millisecond bursts. According to (14), the maximum growth rate varies as U^{-2} , and hence Γ_{\max} can be increased by reducing the thermal spread of the distribution.

The growth rate must be sufficiently high to give sub-

stantial growth in the duration (≈ 10 ms) of the S bursts. Assuming that at least 10 e-foldings of growth are required for observable bursts [Hewitt et al., 1982], the growth rate must exceed the threshold growth rate, Γ_1 , for effective growth, with $\Gamma_{\max} \gtrsim \Gamma_1 = 1000 \text{ s}^{-1}$. The limit on Γ_1 is weaker for L bursts due to their longer duration. The longer timescale of the L bursts implies that a lower growth rate (lower Γ_1) is required to produce them.

Another constraint on the required growth rate is due to the bandwidth $\Delta\omega$. The inhomogeneous structure of the magnetic field implies a change in the cyclotron frequency with distance. The total change in Ω_e over the path length required for substantial growth must not exceed the bandwidth $\Delta\omega$. This leads to the second condition [Hewitt et al., 1982],

$$\Gamma_{\max} \gtrsim \Gamma_2 = \frac{10c}{L}, \quad (22)$$

corresponding to 10 e-foldings over the characteristic growth length, $L = (\Delta\omega/\Omega_e)R_J$, with R_J the radius of Jupiter. This constraint applies both to the S bursts and the L bursts.

In Figure 4 the maximum growth rate Γ_{\max} and the constraints due to the timescale of the bursts ($\Gamma > \Gamma_1$), and the bandwidth ($\Gamma > \Gamma_2$) are plotted as functions of U for the same parameters as in Figure 1 ($u_d = 0.5$, $j = 2$), where Γ_{\max} and $\Delta\omega$ are determined from the expressions derived in section 3. The value $u_d = 0.5$ is chosen to be consistent with the results from section 4.1 (see Table 1). The number density of electrons is chosen to be $n_e = 5 \times 10^6 \text{ m}^{-3}$, which is the upper limit implied by the requirement that mode coupling be strong, so that the elliptical polarization is preserved, between the source and the observer [Melrose and Dulk, 1991]. The magnetic field in the source region is assumed to be $B = 1 \times 10^{-3} \text{ T}$, determined from the observed frequency, with $w \approx \Omega_e$. The effects of varying these parameters are discussed below. The regions in Figure 4 where the growth rate is too small to satisfy the constraints ($\Gamma_{\max} > \Gamma_1$, $\Gamma_{\max} > \Gamma_2$) are shaded. From Figure 4, it is clear that the dominant constraint is the one $\Gamma > \Gamma_1$, which requires, for the S bursts, $U \lesssim 0.1$. For

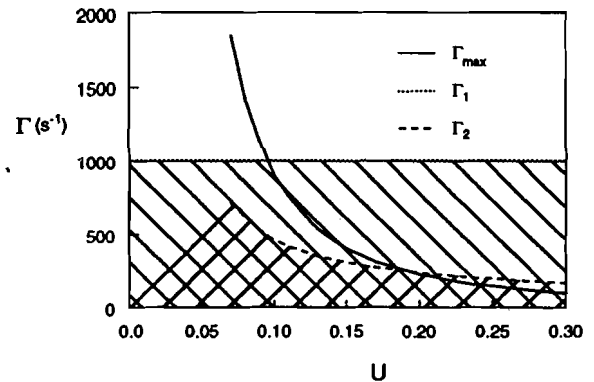


Figure 4. Maximum growth rate Γ_{\max} and constraints Γ_1 and Γ_2 plotted as functions of U . These constraints are satisfied for $U \lesssim 0.1$, with $u_d = 0.5$ and $j = 2$.

the L bursts, Γ_1 is negligible, and $\Gamma_{\max} > \Gamma_2$ requires $U \lesssim 0.2$.

The observed bandwidth is typically 50 kHz for the millisecond bursts [Dulk et al., 1991.1, although much narrower bandwidths have been observed, typically a few kilohertz [Ellis, 1982]. A bandwidth of 50 kHz corresponds to $\Delta(\omega/\Omega_e) \approx 3 \times 10^{-4}$. From the relations (15) and (16), $\Delta(\omega/\Omega_e) \approx 3 \times 10^{-4}$ requires $U \approx 3 \times 10^{-4}$ (with an angular range $\Delta\theta \approx 0.05^\circ$). Hence, the observed bandwidth constraint suggests much smaller distribution widths for the S bursts than due to the constraints Γ_1 and Γ_2 . An alternative explanation for the small observed bandwidth is short-scale structures in the source region [cf. Robinson, 1991a, b], of characteristic length $l = (\Delta\omega/\omega)R_J$. The small-scale structures correspond to regions in which the plasma conditions favor growth of the S bursts. The small bandwidth corresponds to the small spatial region in which the growth occurs. This would allow widths of $U \approx 0.1$ to produce the small observed bandwidths. For the L bursts the wider bandwidth and larger angular range (observed to be $\Delta\theta \approx 1^\circ$ [Dulk, 1967]) imply larger distribution widths. The bandwidth of the L bursts would be unaffected by the above mentioned small-scale structures if the conditions for growth for these bursts were less sensitive to inhomogeneities in the plasma.

4.3. Effect of Variation of the Distribution Function Parameters

In section 4.2 the limits placed on the characteristic width U of the distribution assume particular values for the number density of the electrons and for the anisotropy (in $u_{\parallel} - u_{\perp}$ space) of the distribution func-

tion (j dependence). Here the effect of varying these parameters is investigated. The drift velocity is fixed from the observed elliptical polarization (see section 4.1).

Number density. The dependence of the maximum growth rate (see Appendix B) on the number density of electrons is

$$\Gamma_{\max} \propto \omega_p^2 \propto n_b. \quad (23)$$

As n_b is decreased from $n_b = 5 \times 10^6 \text{ m}^{-3}$, the Γ_{\max} curve in Figure 4 moves to lower values, while the constraints Γ_1 and Γ_2 remain unchanged. This implies that at lower number densities, smaller values of U are required to attain acceptable growth rates.

Anisotropy of the distribution. The perpendicular displacement of the peak of the distribution function satisfies $u_{\perp} = \sqrt{2j}U$, so that for fixed U , the variable j controls the perpendicular displacement of the distribution function in $u_{\parallel} - u_{\perp}$ space. For higher j the electrons in the distribution function are at higher velocities (and energies) so that the maximum growth rate curve in Figure 4 moves to higher Γ . The maximum allowable value of U increases, because the Γ_1 constraint curve is unaffected. As j increases, $\Delta\omega$ and $\Delta\theta$ increase for fixed U .

5. Geometry of the Emission Region

Previous models for Io-related Jovian decametric radiation, while successfully explaining the beaming of the radiation, cannot explain the elliptical polarization from those subsources for which the observed axial ratio ($|T| < 1$) is relatively large, cf. Table 1. The assumption made in this paper is that the elliptical polarization is intrinsic to the emission mechanism of ECME, in which case the simplest theory implies emission (cone opening) angles $\theta \lesssim 50^\circ$. However, these angles appear incompatible with the source geometry. For an observer at Earth to detect the emission, the edge of the hollow emission cone must be directed toward the Earth. Because the Earth-Jupiter distance far exceeds the scale size of the source (of order R_J), this is equivalent to the condition that the angle between the cone axis (which is tangential to the field line at the point of emission) and the vector directed toward the Earth is equal to the angle of emission. A simplified representation of the source geometry is shown in Figure 5, with possible emission cones lying on the Io flux tube. For an arbitrary phase of Io the minimum angle between the cone axis and the vector directed towards the Earth is obtained when the cone axis is oriented parallel to the equatorial plane, as shown in Figure 5. Consider the geometry for the Io-B and Io-D emission, where Io's phase is in the range $60^\circ - 120^\circ$. Even when the cone axis is oriented parallel to the equatorial plane, angles of emission $\theta > 60^\circ$ are required to observe the radiation at Earth. The tilt of the magnetic axis affects this argument by at most 10° . Hence angles of emission of $\theta \lesssim 50^\circ$ are inconsistent with the viewing geometry. A comparison of the angles of emission inferred from

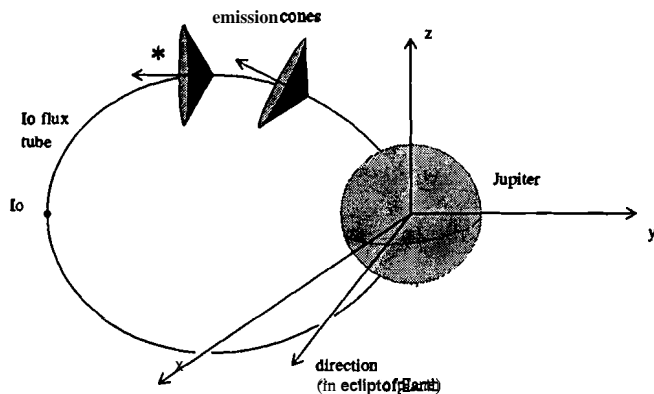


Figure 5. Simplified representation of the source geometry, assuming a dipolar magnetic field, and ignoring the 10° tilt of the Jovian magnetic axis. The Jovian north pole is aligned with the z axis and the x - y plane corresponds to the ecliptic plane. Both Io and the vector pointing towards the Earth lie in the ecliptic plane. Two possible emission cones (which lie on the Io flux tube) are shown for emission from the northern hemisphere. The minimum angle between the cone axis and the direction of the Earth occurs when the cone axis is oriented parallel to the ecliptic plane (i.e., for the emission cone marked by an asterisk).

the source geometry and the angles of emission determined from the observed axial ratios (using the relation $T \approx \cos \theta$) is discussed by Leblanc et al. [1994]. This successfully predicts the source positions, except for the left-hand polarized Io-C source, but cannot account for the elliptical polarization.

The standard model, which predicts angles of emission $70^\circ - 90^\circ$ [Goldstein and Goertz, 1983] is more consistent with the viewing geometry (but does not predict the elliptical polarization). How this inconsistency is to be resolved is unclear. One possible resolution is that the Jovian magnetic field lines do not lie in meridional planes, due to higher order moments in the magnetic field [Baganel and Leblanc, 1988]. This can create a relative phase difference between Io and the source region, allowing for smaller angles between the cone axis and the direction of the Earth, and hence smaller emission angles. However this depends on the longitude of Jupiter and is unlikely to work over the full range of longitude for which the emission is observed (M 90° for each source). Alternatively, the problem may lie with the current assumed model for the source geometry. For example, the source region may not necessarily lie within the magnetic flux tube passing through Io. Finally, if no other resolution is found, this geometric inconsistency may require a new approach to the operation of electron cyclotron maser emission in the Jovian magnetosphere.

6. Summary

Recent observations of Jupiter's decametric radio emission have shown that it is intrinsically elliptically polarized. The polarization is characterized by the axial ratio T , which has different values, depending on the particular subsource. The existing theory for ECME assumes $v \ll c$, where v is the mean speed of the electrons, and predicts the relation $T \approx \cos \theta \approx v/c$, implying small axial ratios (linear polarization) and angles of emission close to 90° . In this paper we extend this theory to a streaming distribution of mildly relativistic electrons with mean velocity v_d along the magnetic field lines, in order to explain the observed elliptical polarization. The results of this analysis are as follows:

1. In $u_{\parallel} - u_{\perp}$ space the resonance ellipse for maximum growth (corresponding to the observed emission) is centered beneath the peak of the electron distribution function.

2. This yields the approximate relations between the mean drift velocity and the angle of emission, $v_d/c \approx \cos \theta / (1 + \cos^2 \theta)$, and between the axial ratio and the angle of emission, $T \approx \cos^3 \theta$.

3. Using these relations, the observed elliptical polarization is consistent with a distribution of electrons streaming with a mean velocity $v_d \approx 0.5c$ along the field lines, with $\theta \lesssim 50^\circ$ (see Table 1). While this model is consistent with the elliptical polarization of Jovian decametric radiation, these angles of emission are inconsistent with the viewing geometry.

4. The other distribution parameters are constrained

by the observed timescale, bandwidth and angular range of the bursts. Assuming that at least 10 e-foldings are required for observable emission, the known timescale of the S bursts constrain the width U of the distribution, with $U \lesssim 0.1$. The observed bandwidth for the S bursts, $\Delta \omega \approx 50$ kHz further constrains the width, with $U \approx 3 \times 10^{-4}$. A possible explanation for the small observed bandwidths is if the growth only occurs within short scale structures in the emission region, allowing larger values of U (than $U \approx 3 \times 10^{-4}$). The longer timescales, wider bandwidths and larger angular ranges of the L bursts from the same Io-related source imply broader electron distributions for these bursts, with an upper limit $U \lesssim 0.2$. The perpendicular anisotropy of the distribution (controlled by the parameter j) is effectively a free parameter in this model, where an increase in j corresponds to an increase in the free energy in the distribution, corresponding to an increase in the growth rate.

Physical models for the acceleration of the electrons to produce such streaming distributions have been postulated [Melrose and Dulk, 1993]. The possibilities include acceleration through the potential due to the motion of Io through the Jovian magnetosphere, or upward acceleration due to a parallel electric field at the Jovian ionosphere, both which contain difficulties. Whichever model applies must be able to account for the source-dependent emission, and in particular, the differences in the emission from the northern and southern hemispheres. In addition, if this explanation for the elliptical polarization is correct, the geometry that allows an observer at Earth to detect the radiation needs to be identified.

Appendix A: Expression for the Growth Rate

The final form of the growth rate is

$$\Gamma(\omega, \theta) = -A_j \alpha^2 \text{Im} \left\{ j! \frac{j \Omega_e}{\omega} \mathcal{F}_{j+\frac{1}{2}}(b, a^2) - (1 - n_{\parallel} u_d) (j+1)! \mathcal{F}_{j+\frac{1}{2}}(b, a^2) \right\}, \quad (\text{A1})$$

where a , b , α , and A_j are defined by (with K_M the longitudinal part of the polarization vector)

$$a = \frac{\cos \theta - u_d}{\sqrt{2} U}, \quad (\text{A2})$$

$$b = \frac{1 - \cos \theta u_d - \Omega_e / \omega + u_d^2 / 2}{U^2}, \quad (\text{A3})$$

$$\alpha = (\cos \theta - u_d) T_M + \sin \theta K_M + \Omega_e / \omega, \quad (\text{A4})$$

$$A_j = \frac{2\omega \omega_p^2 R_M}{2\Omega_e^2 (1 + T_M^2) j! U^2}. \quad (\text{A5})$$

Note that the above formula only applies for emission close to the cyclotron frequency, with the axial ratio (for gyroemission) $T \approx \cos \theta$ and the ratio of electric to total energy $R = 1/2$. The method for numerically evaluating the Shkarofsky functions [Shkarofsky, 1966] is discussed by Willes and Robinson [1994].

Appendix B: Semiquantitative expression for maximum growth rate

The predetermined center and radius of the resonant circle satisfy,

$$u_0 = u_d, \quad u_R = U\sqrt{2j}. \quad (\text{B1})$$

The integration in (5) is performed by transforming to polar coordinates in the $u_{\parallel} - u_{\perp}$ plane, with

$$u_{\parallel} - u_d = u \cos \phi, \quad u_{\perp} = u \sin \phi, \quad (\text{B2})$$

so that,

$$\int d^3u = 2\pi \int_0^{\infty} du \int_0^{\pi} d\phi u^2 \sin \phi. \quad (\text{B3})$$

The delta function satisfies,

$$\delta(u^2 - u_R^2) = \delta((u - u_R)(u + u_R)) = \frac{1}{2u_R} \delta(u - u_R). \quad (\text{B4})$$

The exponentials in the distribution function satisfy

$$\left[\frac{-\{(u_{\parallel} - u_d)^2 + u_{\perp}^2\}}{2U^2} \right] \\ = \exp \left[\frac{-\{u_R^2 \cos^2 \phi + u_R^2 \sin^2 \phi\}}{2U^2} \right] = \exp[-j]. \quad (\text{B5})$$

The integrals that then need to be evaluated are of the form [Gradshteyn and Ryzhik, 1980, p. 373]

$$\int_0^{\pi} d\phi \sin^{2n+1} \phi = \frac{2^{2n+1} (n!)^2}{(2n+1)!}. \quad (\text{B6})$$

The final form (14) of the semiquantitative growth rate is then obtained.

Acknowledgments. The authors thank G. A. Dulk for careful and constructive comments and for providing preprints of unpublished observations. This work was supported by an Australian Research Council Queen Elizabeth II Fellowship, an Australian Postgraduate Research Award and by the Research Center for Theoretical Astrophysics. The Editor thanks G. A. Dulk and another referee for their assistance in evaluating this paper.

References

- Baganel, F., and Y. Leblanc, **Io's Alfvén wave pattern and the Jovian decametric arcs**, *Astron. Astrophys.*, 197, 311, 1988.
- Barrow, C. H., **Polarization of the Io-C radio emission from Jupiter**, *J. Geophys. Res.*, 97, 8169, 1992.
- Carr, T. D., M. D. Desch, and J. K. Alexander, **Phenomenology of magnetospheric radio emissions**, in *Physics of the Jovian magnetosphere*, edited by A. J. Dessler, p. 226, Cambridge University Press, New York, 1983.
- Dory, R. A., G. E. Guest, and E. G. Harris, **Unstable electrostatic plasma waves propagating perpendicular to a magnetic field**, *Phys. Rev. Lett.*, 14, 131, 1965.
- Dulk, G. A., **Apparent changes in the rotation rate of Jupiter**, *Icarus*, 7, 173, 1967.
- Dulk, G. A., Y. Leblanc, and A. Lecacheux, **The complete polarization state of Io-related radio storms from Jupiter: a statistical study** *Astron. Astrophys.*, in press, 1994.
- Dulk, G. A., A. Lecacheux, and Y. Leblanc, **The complete polarization state of a storm of millisecond bursts from Jupiter**, *Astron. Astrophys.*, 253, 292, 1991.
- Ellis, G. R. A., **Observations of the Jupiter S-bursts between 3.2 and 32 MHz**, *Aust. J. Phys.*, 35, 165, 1982.
- Goldreich, P., and D. Lynden-Bell, **Io, a Jovian inductor**, *Astrophys. J.*, 156, 59, 1969.
- Goldstein, M. L., and C. K. Goertz, **Theories of radio emissions and plasma waves, in Physics of the Jovian magnetosphere**, edited by A. J. Dessler, p. 317, Cambridge University Press, New York, 1983.
- Goldstein, M. L., and J. R. Thieman, **The formation of arcs in the dynamic spectra of Jovian decameter bursts**, *J. Geophys. Res.*, 86, 8569, 1981.
- Gradshteyn, I. S., and I. M. Ryzhik, **Table of integrals, series and products**, Academic Press, New York, 1980.
- Hewitt, R. G., D. B. Melrose, and K. G. Rönnmark, **A cyclotron theory for the beaming pattern of Jupiter's decametric radio emission**, *Proc. Astron. Soc. Aust.*, 4, 226, 1981.
- Hewitt, R. G., D. B. Melrose, and K. G. Rönnmark, **The loss-cone driven electron-cyclotron maser**, *Aust. J. Phys.*, 35, 447, 1982.
- Leblanc, Y., G. A. Dulk, and F. Baganel, **The elliptical polarization of Jupiter's decametric radio emission and the origin of the radiation**, *Astron. Astrophys.*, in press, 1994.
- Lecacheux, A., A. Boischoit, M. Y. Boudjada, and G. A. Dulk, **Spectra and complete polarization state of two, Io-related, radio storms from Jupiter**, *Astron. Astrophys.*, 251, 339, 1991.
- Le Quéau, D., and P. Louarn, **Analytical study of the relativistic dispersion: Application to the generation of the auroral kilometric radiation**, *J. Geophys. Res.*, 94, 2605, 1989.
- Melrose, D. B., **Instabilities in Space and Laboratory Plasmas**, Cambridge University Press, New York, 1986.
- Melrose, D. B., and G. A. Dulk, **On the elliptical polarization of Jupiter's decametric radio emission**, *Astron. Astrophys.*, 249, 250, 1991.
- Melrose, D. B., and G. A. Dulk, **Electron cyclotron maser emission at oblique angles**, *Planet. Space Sci.*, 41, 5, 1993.
- Melrose, D. B., K. G. Rönnmark, and R. G. Hewitt, **Terrestrial kilometric radiation: The cyclotron theory**, *J. Geophys. Res.*, 87, 5140, 1982.
- Omidi, N., and D. A. Gurnett, **Growth rate calculations of auroral kilometric radiation using the relativistic resonance condition**, *J. Geophys. Res.*, 87, 2377, 1982.
- Pritchett, P. L., **Relativistic dispersion, the cyclotron maser instability, and auroral kilometric radiation**, *J. Geophys. Res.*, 89, 8957, 1984.
- Robinson, P. A., **Relativistic plasma dispersion functions**, *J. Math. Phys.*, 27, 1206, 1986a.
- Robinson, P. A., **Electron cyclotron waves: dispersion and accessibility conditions in isotropic and anisotropic plasmas**, *J. Plasma Phys.*, 35, 187, 1986b.
- Robinson, P. A., **Thermal effects on parallel-propagating electron cyclotron waves**, *J. Plasma Phys.*, 37, 149, 1987.
- Robinson, P. A., **Electron-cyclotron maser emission in solar microwave spike bursts**, *Sol. Phys.*, 134, 299, 1991a.
- Robinson, P. A., **Effects of turbulence on the electron cyclotron-maser mechanism for solar microwave spike bursts**, *Sol. Phys.*, 136, 343, 1991b.
- Shkarofsky, I. P., **Dielectric tensor in Vlasov plasmas near cyclotron harmonics**, *Phys. Fluids*, 9, 561, 1966.
- Strangeway, R. J., **Wave dispersion and ray propagation in a weakly relativistic electron plasma: Implications for the generation of auroral kilometric radiation**, *J. Geophys. Res.*, 90, 9675, 1985.

- Strangeway, R. J.**, On the applicability of relativistic dispersion to auroral zone electron distributions, *J. Geophys. Res.*, 91, 3152, 1986.
- Warwick, J.W.**, and G.A. Dulk, Faraday rotation on **decametric** radio emissions from Jupiter, *Science*, 145, 380, 1964.
- Willes, A. J.**, and P. A. Robinson, Electron cyclotron maser emission from streaming distributions, *J. Plasma Phys.*, in press, 1994.
- Winglee, R. M.**, Interrelation between azimuthal bunching and semirelativistic maser cyclotron instabilities, *J. Plasma Phys.*, 25, 217, 1983.
- Winglee, R. M.**, Effects of a finite plasma temperature on electron-cyclotron maser emission, *Astrophys. J.*, 291, 160, 1985.
- Wu, C. S., and L. C. Lee, A theory of the terrestrial kilometric radiation, *Astrophys. J.*, 230, 621, 1979.
-
- D. B. Melrose, P. A. Robinson, and A. J. Willes, Department of Theoretical Physics and Research Center for Theoretical Astrophysics, School of Physics, University of Sydney, NSW 2006, Australia. (e-mail: willes@physics.su.oz.au)

(Received October 15, 1993; revised April 20, 1994; accepted July 13, 1994.)